Hydrothermal Synthesis and Properties of Mixed Conducting $Ce_{1-x}Tb_xO_{2-\delta}$ Solid Solutions

P. Shuk,[†] M. Greenblatt,*[,†] and M. Croft[‡]

Department of Chemistry, Rutgers, the State University of New Jersey, 610 Taylor Rd, Piscataway, New Jersey 08854-8087, and Department of Physics and Astronomy, Rutgers, the State University of New Jersey, Piscataway, New Jersey 08854-8019

Received September 28, 1998. Revised Manuscript Received November 17, 1998

The structure, thermal expansion coefficients, and ionic and electronic conductivities of $Ce_{1-x}Tb_xO_{2-\delta}$ ($x = 0-0.30$) solid solutions, prepared hydrothermally for the first time, were investigated. The uniformly small particle size (33−40 nm) of the hydrothermally prepared materials allows sintering of the samples into highly dense ceramic pellets at 1300−1400 °C, a significantly lower temperature, compared to that at 1600−1650 °C required for samples prepared by solid-state techniques. X-ray absorption near edge spectroscopy was used for the identification of Tb^{3+}/Tb^{4+} ions. The maximum of total conductivity was found at $x = 0.25$ ($\sigma_{700°C} = 2.1 \times 10^{-2}$ S/cm, $E_a = 0.49$ eV) with electronic contribution to the total conductivity around ∼50% at 600−700 °C. The conductivity becomes more ionic with decreasing Tb substitution. The thermal expansion coefficients, determined from high-temperature X-ray diffraction data, are 11.7×10^{-6} K^{-1} for CeO_2 and slowly decrease with increasing Tb substitution (10.8×10^{-6} K^{-1} at $x = 0.30$).

Introduction

The solid electrolyte is a key component of solid-state electrochemical devices, which are increasingly important for applications in energy conversion, chemical processing, sensing, and combustion control.[1−3] High oxide ion conducting solid electrolytes based on ZrO_2 (zirconia) have been extensively investigated and reviewed in the past as well as successfully applied in various electrochemical devices.[4−8] Although stabilized zirconia is considered to be the most reliable solid electrolyte so far, many studies have been made on other solid electrolytes as alternatives to zirconia, e.g. Bi_2O_3[9−11] and CeO_2[12] based materials, to increase the efficiency of the electrochemical device and decrease the application temperature. In the past several years, CeO_2-based materials have been intensely investigated as catalysts, structural and electronic promoters of heterogeneous catalytic reactions, and oxide ion conducting solid electrolytes in electrochemical cells.[12−14] For the last of these applications, relatively high ionic conductivity of the solid electrolyte is required for device performance. The oxygen vacancy ($V_O^{\bullet\bullet}$), concentration, and concomitant oxide ion conductivity in cerium oxide can be increased by substitution of a lower-valent metal ion (e.g. M^{3+}) for cerium:

$$2CeO_2 \xrightarrow{2MO_{1.5}} 2M_{Ce}' + V_O^{\bullet\bullet} + {}^1/_2O_2 \qquad (1)$$

In the past, many investigations have been carried out on various aspects of ceria solid electrolytes mostly prepared by conventional ceramic methods.[12] However, the preparation temperature or time needed to obtain a homogeneous solid solution depends significantly on the particle size of the starting materials. Yttrium- and samarium-doped ceria solid electrolytes have been successfully prepared by a hydrothermal method, providing low-temperature preparation and morphological control of ultrafine particles of uniform crystallite dimension.[15,16] Recently we have shown that solid solutions of $Ce_{1-x}Sm_xO_{2-x/2}$ and $Ce_xCa_xO_{2-x}$ can be hydrothermally prepared in a wide substitution range of Sm or Ca.[17]

* To whom correspondence should be addressed. E-mail: martha@rutchem.rutgers.edu.
† Department of Chemistry.
‡ Department of Physics and Astronomy.

(1) Takahashi, T.; Kozawa, A. (Eds.) *Application of Solid Electrolytes*; JEC Press: Ohio, 1980.
(2) Takahashi, T. (Ed.) *High Conductivity Solid Ionic Conductors*; World Scientific: Singapore, 1989.
(3) Göpel, W.; Jones, T. A.; Kleitz, M.; Lundström, I.; Seiyama, T. (Eds.) *Chemical and Biochemical Sensors*; VCH: Weinheim, Germany, 1991/1992; Vol. 2, 3.
(4) Etsell, T. H.; Flengas, S. N. *Chem. Rev.* **1970**, *70*, 339.
(5) Steele, B. C. H. *Sci. Ceram.* **1980**, *10*, 1.
(6) Subbarao, E.; Maiti, H. S. *Solid State Ionics* **1984**, *11*, 317.
(7) Steele, B. C. H. *J. Power Sources* **1994**, *49*, 1.
(8) Badwal, S. P. S., Ed. *Science and Technology of Zirconia*; Technomic: Lancaster, U.K., 1993.
(9) Takahashi, T.; Iwahara H. *Mater. Res. Bull.* **1978**, *13*, 1447.
(10) Azad, A. M.; Larose, S.; Akbar, S. A. *J. Mater. Sci.* **1994**, *29*, 4135.
(11) Shuk, P.; Wiemhöfer, H.-D.; Guth, U.; Göpel, W.; Greenblatt, M. *Solid State Ionics* **1996**, *89*, 179.
(12) Inaba, H.; Tagawa, H. *Solid State Ionics* **1996**, *83*, 1.
(13) Trovarelli, A. *Catal. Rev.−Sci. Eng.* **1996**, *38*, 439.
(14) Gellings, P. J.; Bouwmeester, H. J. M. *Catal. Today* **1992**, *1*, 1.
(15) Zhou, Y. C.; Rahaman, M. N. *J. Mater. Res.* **1993**, *8*, 1680.
(16) Yamashita, K.; Ramanujachary, K. V.; Greenblatt, M. *Solid State Ionics* **1995**, *81*, 53.
(17) Huang, W.; Shuk, P.; Greenblatt, M. *Chem. Mater.* **1997**, *9*, 2240.

10.1021/cm980682d CCC: $18.00
Published on Web 01/05/1999

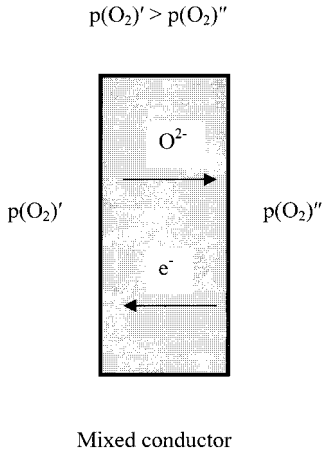

Figure 1. Schematic oxygen membrane with mixed conducting oxide.

While past efforts in solid-state ionics focused on expanding the electrolytic domain of oxide ion conducting solid electrolytes for application in solid oxide fuel cells (SOFC) or sensors, more recently efforts began to introduce enhanced electronic conduction in high ion conductive matrixes to develop mixed conductors for oxygen membrane application.[18] For this application equally high electronic and ionic conductivities are required to achieve maximum oxygen flux through the membrane needed for oxygen separation.[18,19] The driving force for overall oxygen transport is the differential chemical potential or partial pressure of oxygen applied across the membrane (Figure 1). Oxide ions will migrate selectively through the oxygen membrane when the membrane is gastight. The flux of oxide ions is charge compensated by a simultaneous flux of electronic charge carriers. At the lower-pressure side, the oxide ions part with their electrons and recombine to form oxygen molecules, which are released in the permeate stream. The flux at a given total conductivity is maximum when the ionic and electronic conductivities are equal.

Teraoka et al.[20] were the first to report, in addition to very high electronic conductivity, high oxide ion conductivity and associated high oxygen permeability in perovskite-type materials. Presently, extensive research in being conducted on acceptor-doped perovskite oxides $Ln_{1-x}A_xCo_{1-y}B_yO_{3-\delta}$ (A = Ca, Sr, Ba; B = Fe, Cu, Ni, Mn).[18] The structural and chemical integrity of the cobaltites as well as their very high thermal expansion coefficients ($>20 \times 10^{-6}$ K^{-1}) are limiting factors for their application as oxygen membranes.

More reliable oxygen membranes may be developed on the basis of fluorite-type oxide ion conducting solid electrolytes, which are more stable and have considerably smaller thermal expansion coefficients ($\sim 10^{-5}$ K^{-1}), if equally high electronic conductivity can be introduced into the fluorite matrix. Takasu et al.[21] and more recently Nauer et al.[22] investigated mixed (oxide ion and electron) conducting praseodymium-substituted ceria, $Ce_{1-x}Pr_xO_{2-\delta}$, for application as cathode materials for SOFC. Takasu et al. reported solid solution formation with the fluorite structure up to $x < 0.70$, while Nauer et al. were able to prepare a single fluorite-phase with $x \leq 0.3$. Both of these studies indicated high, activated, mixed conductivity for samples of $Ce_{1-x}Pr_xO_{2-\delta}$ with the highest Pr content (e.g. $\sigma_{600°C} \sim 10^{-2}$ S/cm for $Ce_{0.6}Pr_{0.4}O_{1.8+\delta}$[21]) with large contributions to the conductivity by electrons. Recently we have shown that the oxygen permeability, $J(O_2)$, of the Pr substituted ceria [$J(O_2) = 1.9 \times 10^{-10}$ mol/s·cm for $Ce_{0.70}Pr_{0.30}O_{1.85+\delta}$ at 700 °C] is close to the oxygen permeability value of the mixed conductors based on the best conductive bismuth oxide solid electrolytes.[23] Another rare earth element, Tb, like Pr, is known to have mixed valency at atmospheric pressure and contribution to electronic conductivity in oxide ion conducting solid electrolytes based on Bi_2O_3.[24]

In this paper we present a systematic study of the structure, ionic and electronic conductivities, and thermophysical properties of terbium-substituted ceria solid solutions, $Ce_{1-x}Tb_xO_{2-\delta}$ prepared for the first time hydrothermally.

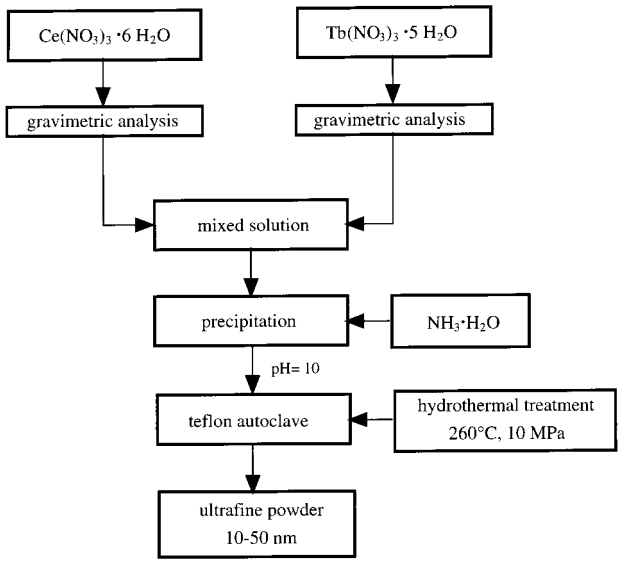

Figure 2. Flow diagram of the hydrothermal synthesis.

Experimental Section

Solid solutions of $Ce_{1-x}Tb_xO_{2-\delta}$ ($x = 0-0.30$) were synthesized by the hydrothermal method as previously reported for the Sm- and Ca-doped ceria solid electrolytes.[17] The appropriate quantities of cerium(III) nitrate hexahydrate ($Ce(NO_3)_3 \cdot 6H_2O$, 99.9% Aldrich) and terbium(III) nitrate pentahydrate ($Tb(NO_3)_3 \cdot 5H_2O$, 99.9% Alfa) were dissolved separately in water, mixed, and coprecipitated with ammonium hydroxide at pH = 10. The precipitated gels were sealed into Teflon-lined steel autoclaves and hydrothermally treated at 260 °C for 10 h (Figure 2). The autoclaves were quenched at 260 °C and the crystallized powder products were repeatedly washed with deionized water and dried in air at room temperature.

The room/high-temperature powder X-ray diffraction patterns (PXD) of the ultrafine powders were obtained with a SCINTAG PAD V diffractometer equipped without/with a high-temperature attachment with monochromatized Cu Kα

(18) Gellings, P. J., Bouwmeester, H. J.-M., Eds. *Solid State Electrochemistry*; CRC Press: New York, 1997.
(19) Möbius, H.-H. *Extend. Abstr. 37th Meeting ISE;* Vilnius, USSR, Aug 24−31, 1986; Vol. 1, p 136.
(20) Teraoka, Y.; Zhang, H. M.; Furukawa, S.; Yamazoe, N. *Chem. Lett.* **1985**, 1743.
(21) Takasu, Y.; Sugino, T.; Matsuda, Y. *J. Appl. Electrochem.* **1984**, *14*, 79.
(22) Nauer, M.; Fticos, Ch.; Steele, B. C. H. *J. European Ceram. Soc.* **1994**, *14*, 493.
(23) Shuk, P.; Greenblatt, M. *Solid State Ionics* **1998**, *116*, 000.
(24) Shuk, P.; Jacobs, S.; Möbius, H.-H. *Z. Anorg. Allg. Chem.* **1985**, *524*, 144.

radiation at a 2θ scan of 0.5°/min. Cell parameters were calculated by fitting the observed reflections with a least-squares program. The reflection from the (422) plane was used for the determination of average crystallite size. The average crystallite size, D, of the hydrothermally prepared powders was calculated from the Scherrer formula:

$$D = \frac{0.9\lambda}{\beta \cos \theta} \tag{2}$$

where λ is the wavelength of the X-rays, θ is the diffraction angle, $\beta = \sqrt{(\beta^2_m - \beta^2_s)}$, the corrected halfwidth of the observed halfwidth, β_m, of the (422) reflection in samples of $Ce_{1-x}Tb_xO_{2-\delta}$, and β_s is the halfwidth of the (422) reflection in a standard sample of CeO_2 ($D \sim 100$ nm). Differential thermal analysis (DTA) and thermogravimetric analysis (TGA) measurements were carried out in the temperature range 25−750 °C with a TA Instruments DSC 2910 and TGA 2050 with a heating and cooling rate of 1 °C/min.

The powder samples were pelletized and sintered at 1300−1400 °C for 4 h with a programmed heating and cooling rate of 5 °C/min. The sintered samples were over 95−97% of the theoretical density in all cases. The microstructure of sintered samples was studied with an atomic force microscope (AFM, QScope Model 250, Quesant Instrument Corporation, CA). The electrical conductivity of the materials was measured on a sintered ceramic pellet. Silver paste was painted onto two faces of the pellets, using GC electronics paste. The sample was then dried and fired at 650 °C. The ionic conductivity measurements were performed by the complex impedance method at frequencies ranging from 0.1 Hz to 65 kHz (Solartron 1280 frequency response analyzer) on isothermal plateaus 1 h long, in air on heating and cooling every 200 °C up to 700 °C. To determine the oxide ion transfer numbers, the EMF of the following oxygen concentration cell was measured:

$$p(O_2)^a, O_2, Ag \mid Ce_{1-x}Tb_xO_{2-\delta} \text{ sample} \mid Ag, O_2, p(O_2)^c \tag{3}$$

If the conduction in ceria solid solutions is predominantly ionic, the theoretical EMF (E_{th}) is given by the Nernst equation

$$E_{th} = \frac{RT}{4F} \ln \frac{p(O_2)^c}{p(O_2)^a} \tag{4}$$

where R, T, and F are the gas constant, the temperature, and the Faraday constant, respectively, and $p(O_2)^a = 1.01 \times 10^5$ Pa and $p(O_2)^c = 0.21 \times 10^5$ Pa are oxygen partial pressures at the anode (pure oxygen) and cathode (air), respectively. If the specimen has some electronic conduction, the measured EMF (E) will be lower than E_{th} because of the discharge of the electrochemical cell due to the electronic conduction. If the electrodes are sufficiently reversible, the oxide ion transfer numbers, t_i can be calculated as follow

$$t_i = \frac{\sigma_i}{\sigma_i + \sigma_e} = \frac{E}{E_{th}} \tag{5}$$

where σ_i and σ_e are ionic and electronic conductivities, respectively.

The oxygen permeability, $J(O_2)$ (mol/s·cm), was calculated from the electronic and ionic contributions to the total conductivity, σ_{total}, using the Wagner equation:[19]

$$J(O_2) = \frac{RT}{16F^2} t_i(1 - t_i)\sigma_{total} \tag{6}$$

Results and Discussion

The PXD data in Figure 3 show that $Ce_{1-x}Tb_xO_{2-\delta}$, prepared by hydrothermal synthesis for the first time, forms solid solutions with the fluorite structure in the Tb substitution range $x = 0-0.30$ that was investigated. The fluorite-phase evolution of $Ce_{0.70}Tb_{0.30}O_{1.85+\delta}$ in the hydrothermal process as a function of heat-treatment time at 260 °C was examined by PXD. After 20 min of heating, the precipitated product is a fine crystalline powder (~20 nm average particle size) of cerium/terbium solid solution (Figure 4). Further hydrothermal heat treatment increases the crystallinity of the powder, e.g., 30 nm in 40 min, 32 nm in 60 min, and ~35 nm in 12 h.

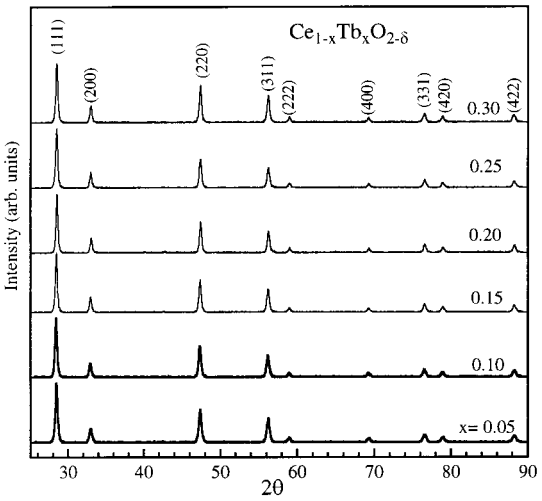

Figure 3. Powder X-ray diffraction patterns of $Ce_{1-x}Tb_xO_{2-\delta}$ solid solutions quenched at 260 °C.

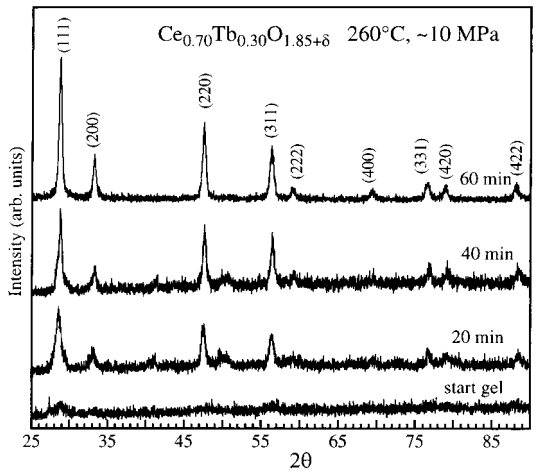

Figure 4. Evolution of the powder X-ray diffraction patterns of a hydrothermally prepared $Ce_{0.70}Tb_{0.30}O_{1.85+\delta}$ solid solution quenched at 260 °C as a function of time.

The unit cell parameter a slowly decreases with increasing Tb content (Figure 5), in good agreement with effective ionic radii considerations ($r_{Ce^{4+}} = 0.111$ nm, $r_{Tb^{4+}} = 0.102$ nm, $r_{Tb^{3+}} = 0.118$ nm; $r_{Tb^{4+}/Tb^{3+}} = 0.110$ nm).[25] It was shown early by Sovestnov et al.[26] that the valence of Tb depends strongly on the history of the sample and decreases in quenched samples and/or increasing Tb concentration in $Ce_{1-x}Tb_xO_{2-\delta}$ solid solutions. The lattice parameters decrease slightly after the 1000 °C anneal (compared to the quenched samples),

(25) Shannon, R. D.; Prewitt, C. T. *Acta Crystallogr.* **1976**, *32A*, 751.
(26) Sovestnov, A. E.; Shaburov, V. A.; Melekh, B. T.; Smirnov, I. A.; Smirnov, Yu. P.; Tyunis, A. V.; Egorov, A. I. *Phys. Solid State* **1994**, *36*, 620.

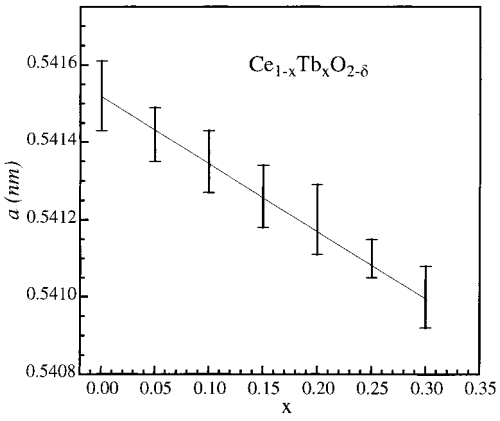

Figure 5. Lattice constants of $Ce_{1-x}Tb_xO_{2-\delta}$ solid solutions as a function of x.

because the Tb^{3+}/Tb^{4+} equilibrium is shifted to Tb^{4+} formation at lower temperatures.[25] The oxygen content in $Ce_{1-x}Tb_xO_{2-\delta}$ depends on the relative ratio of Tb^{4+}/Tb^{3+} (i.e., $\delta \approx [Tb^{3+}]/2$) and therefore increases with decreasing temperature (lower δ values).

The average crystallite size, D, of terbium-substituted ceria powders, calculated by the Scherrer formula from the PXD data, was between 33 and 40 nm (Table 1). The fine, substituted ceria powders were sintered into pellets with apparent densities over 95% of the theoretical value at 1300−1400 °C, whereas ceria solid electrolytes prepared by conventional ceramic techniques require over 1600 °C for sintering.

Temperature-dependent X-ray diffraction measurements show no transformation of the fluorite structure nor phase separation of CeO_2 or $TbO_{1.75}$ (Figure 6), even after annealing at 800−1000 °C for 2 weeks. The lattice constant a increases linearly with temperature (Figure 7); the thermal expansion coefficients determined from these data are 11.8×10^{-6} K^{-1} for CeO_2 and slightly decreases with increasing Tb content to 10.8×10^{-6} K^{-1} for $Ce_{0.70}Tb_{0.30}O_{1.85+\delta}$ (Table 1).

In Figure 8 the AFM topographic image of the $Ce_{0.80}Tb_{0.20}O_{1.90+\delta}$ sample sintered at 1300 °C indicates relatively small particles of uniform size, ∼0.3−1 μm, and very dense microstructure. As expected, these particles are considerably larger than those of the "as-prepared" powder (∼40 nm).

Pure ceria oxide is basically a poor oxide ion conductor ($\sigma_{700°C} = 1.9 \times 10^{-5}$ S/cm). The ionic conductivities are significantly enhanced in $Ce_{1-x}Tb_xO_{2-\delta}$ solid electrolytes (Figure 9) by the substitution of Ce^{4+} by Tb^{3+}, leading to an increase of the oxygen vacancies, $V_O^{\bullet\bullet}$:

$$2CeO_2 \xrightarrow{2TbO_{2-\delta}} 2Tb_{Ce}' + V_O^{\bullet\bullet} + {}^1/_2O_2 \qquad (7)$$

Since terbium is known to have a mixed valence even at atmospheric pressure and room temperature, an equilibrium between Tb^{3+} and Tb^{4+} exists, determined by the temperature and oxygen pressure

$$2Tb_{Tb}' + V_O^{\bullet\bullet} + {}^1/_2O_2 \leftrightarrow 2Tb_{Tb}^{\,x} + O_O^{\,x} \qquad (8)$$

where $Tb_{Tb}' = Tb^{3+}$, $Tb_{Tb}^{\,x} = Tb^{4+}$.

This equilibrium will reduce the expected oxygen vacancy concentration, and the oxide ion conductivity will increase more slowly with increasing Tb substitution than in the Sm- or Ca-substituted ceria systems.[17] The oxide ion conductivity in $Ce_{1-x}Tb_xO_{2-\delta}$ reaches a maximum at 25% substitution (Figure 10). At the same time, with increasing Tb concentration the electronic contribution to the total conductivity increases (Figures 10 and 11), due to the hopping of small polarons between Tb^{3+} and Tb^{4+}. The electronic conductivity exceeds the oxide ion conductivity at $x > 0.25$ (Figure 10).

X-ray absorption near edge spectroscopy (XANES) shows (Figure 12) that at lower Tb substitution in $Ce_{1-x}Tb_xO_{2-\delta}$ ($x = 0.05$) Tb^{3+} is dominant. The Tb-L_3 edge of the standard Tb_4O_7 sample (with a formal Tb valence of 3.5) has very comparable intensities in the Tb^{3+} and Tb^{4+} features. The average Tb valence is indicated by the relative weights of these respective features. The C-feature (Figure 12) has been shown to reflect the rare earth-oxygen ligand shell distance.[27] The C-features in the $Ce_{1-x}Tb_xO_{2-\delta}$ spectra are shifted to lower energy, indicating an expanded Tb−O distance relative to Tb_4O_7.

The spectrum of the $x = 0.05$ compound manifests a single intense feature, indicating an essentially pure Tb^{3+} state. In the $x = 0.3$ spectrum the Tb^{4+} component is appreciably stronger than in the $x = 0.05$ case; however, the Tb^{3+} feature is still dominant. Thus Tb substitutes into these hydrothermally prepared $Ce_{1-x}Tb_xO_{2-\delta}$ materials as Tb^{3+} at lower concentrations, with an increasing Tb^{4+} component at higher Tb concentrations, and, finally, even at $x = 0.3$, Tb^{3+} is still the major component. This behavior is consistent with the association of the initial Tb^{3+} substitution with oxygen vacancies ($V_O^{\bullet\bullet}$) and with the crossover to increasing Tb^{4+} character as the Tb substitution occurs at fully O-coordinated sites at higher x values. The affinity of Tb for the O vacancies is in accord with expectation, in view of the higher redox potential of Tb^{4+} relative to Ce^{4+}. This was confirmed also by the ion transfer number measurements (Figure 11), where only ion conductivity is observed for $Ce_{0.95}Tb_{0.05}O_{2-\delta}$ composition (i.e., no electron transfer between Tb^{4+} and Tb^{3+} ion). With increasing Tb concentration, the electronic contribution to the total conductivity is increasing, due to the motion of the small polarons by a thermally activated hopping mechanism.

Although the trends in the average Tb valence are clear from inspection of the spectra, it is conventional to quantify them with an L_3-valence estimate, v_3.[28] To do so, the replicate Tb^{4+}/Tb^{3+} edge features are each modeled by a Gaussian (for the WL-feature) and an arctangent (for the continuum onset). The centers of the arctangent and the Gaussian are constrained to have the same energy, and the Gaussian area (WL-oscillator strength) is constrained to have the same ratio to the arctangent step height for both of the replicate features. The Gaussian widths, positions, and heights are allowed to vary as well as the replicate feature weights (w_3 and w_4 with $w_3 + w_4 = 1$). Within this fitting procedure the

(27) Jeon, Y.; Lu, F.; Jhans, H.; Shaheen, S.; Liang, G.; Croft, M.; Ansari, P.; Ramanujachary, K.; Hayri, E.; Fine, S.; Li, S.; Feng, X.; Greenblatt, M.; Green, L.; Tarascon, J. *Phys. Rev.* **1987**, *B36*, 3891.

(28) Ramanujachary, K. V.; Sunstrom, J. E.; Fawcett, I.; Shuk, P.; Greenblatt, M.; Croft, M.; Novick, I.; Herber, R. H.; Khalid, S. *Mater. Res. Bull.* **1998**, *34*, 000.

Table 1. Lattice Parameters, Crystallite Sizes, and Electrical Properties of $Ce_{1-x}Tb_xO_{2-\delta}$ Solid Solutions

composition, x =	lattice parameter a (nm)	average crystallite size, D (nm)	conductivity, $\sigma_{700°C}$ (S/cm) (±5%)	activation energy, E_a (eV) (±0.05)	thermal expansion coefficients, TEC
0	0.54152(9)	40	1.9×10^{-5}	1.03	11.8 (3)
0.05	0.54142(7)	40	9.8×10^{-4}	1.2 (>450 °C) 0.37 (<450 °C)	11.7(4)
0.10	0.54135(8)	35	3.0×10^{-3}	1.2 (>450 °C) 0.40 (>450 °C)	11.6(4)
0.15	0.54126(8)	36	3.3×10^{-3}	1.1 (>450 °C) 0.45 (<450 °C)	11.5(4)
0.20	0.54120(9)	38	9.2×10^{-3}	0.76 (>450 °C) 0.46 (<450 °C)	11.4(4)
0.25	0.54110(5)	37	2.1×10^{-2}	0.82 (>450 °C) 0.49 (<450 °C)	11.1(3)
0.30	0.54100(8)	33	1.5×10^{-2}	0.87 (>450 °C) 0.47 (<450 °C)	10.8(4)

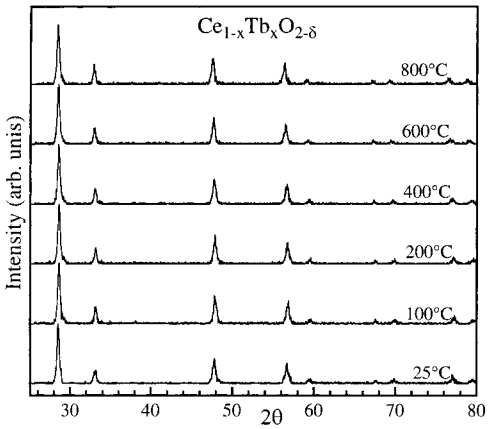

Figure 6. Powder X-ray diffraction patterns of the $Ce_{0.70}Tb_{0.30}O_{1.85+\delta}$ solid solutions as a function of temperature.

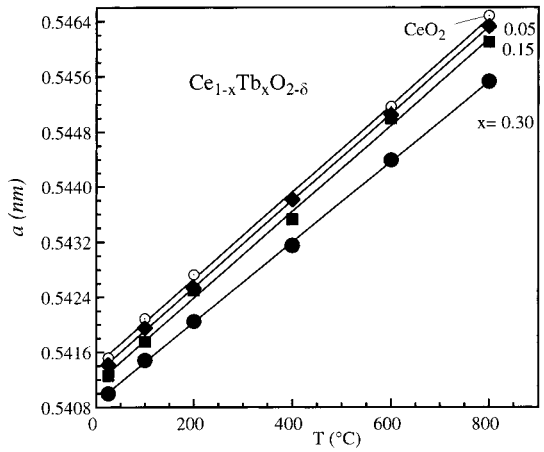

Figure 7. Temperature dependence of the lattice constants of selected ceria solid electrolytes (quenched at 260 °C).

uncertainties in the fitted values of v_3 are ±0.02 or better; however, the choice of a different edge modeling form could lead to systematic changes on the order of ±0.05. The average L_3-valence is defined by $v_3 = 3w_3 + 4w_4$. The results of the fitting process along with the separate Tb^{4+}/Tb^{3+} replicate edge features are shown in Figure 13. Values of L_3-valence estimates have been shown to correlate very well with bond distance estimated valence variations in mixed-valent rare earth compounds. Nevertheless, an exact equality between the values of the formal valence and the L_3-valence estimates need not occur. In this study the agreement between the formal valence of 3.5 and $v_3 = 3.48 \pm 0.02$

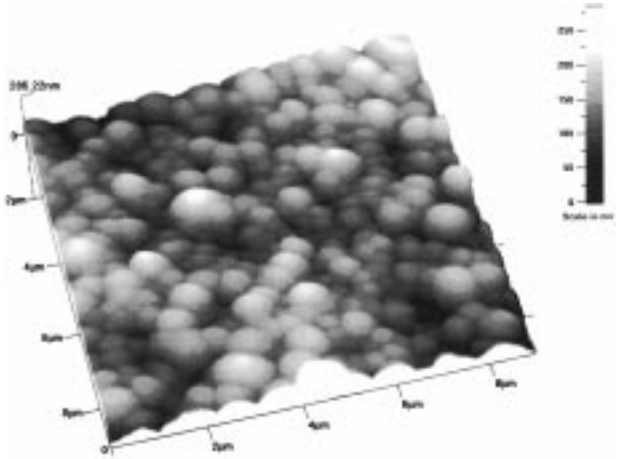

Figure 8. In situ AFM topographic image of a sintered (1300 °C) $Ce_{0.70}Tb_{0.30}O_{1.85+\delta}$ sample.

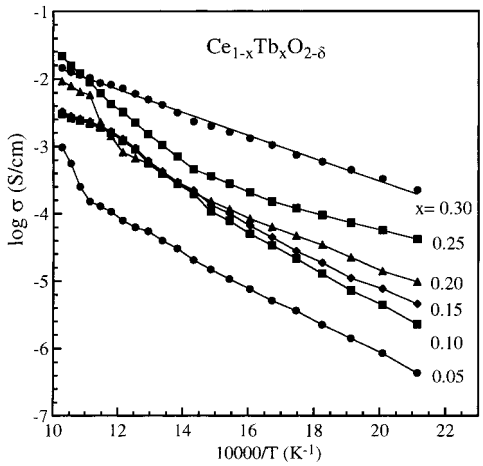

Figure 9. Arrhenius plots of the ionic conductivity of $Ce_{1-x}Tb_xO_{2-\delta}$ solid solutions.

for Tb_4O_7 is encouraging; however, more extensive studies are required before definitive conclusions can be made. The formal valence of 3.0 and 3.26 for Tb was found in $Ce_{1-x}Tb_xO_{2-\delta}$ for $x = 0.05$ and 0.30, respectively.

The oxygen permeability, $J(O_2)$, calculated from ionic and electronic conductivies using Wagner's equation (6) systematically increases with increasing Tb substitution and temperature (Figure 14) and reaches a maximum at $x = 0.25$ [$J(O_2) = 2.9 \times 10^{-10}$ mol/s·cm at 700 °C]. The oxygen permeability is close to that of mixed conductors based on the best conductive bismuth oxide

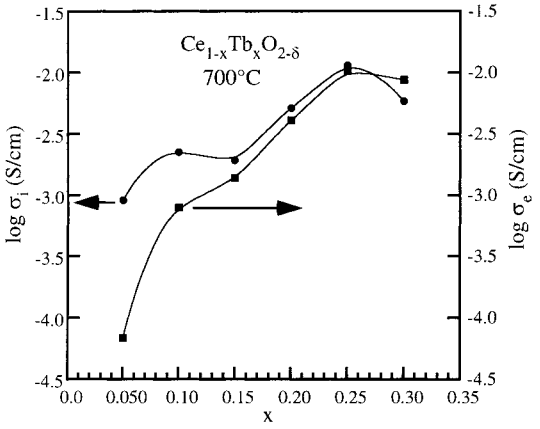

Figure 10. Concentration dependence of the ionic and electronic conductivities of $Ce_{1-x}Tb_xO_{2-\delta}$ solid solutions at 700 °C.

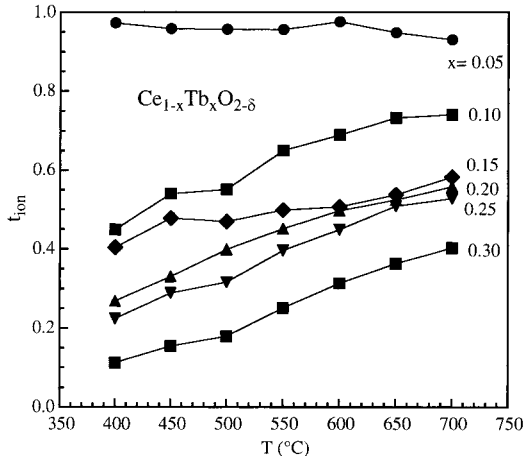

Figure 11. Ionic transference number of $Ce_{1-x}Tb_xO_{2-\delta}$ solid solutions.

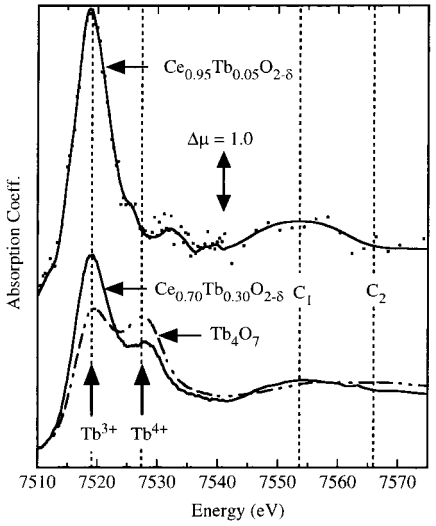

Figure 12. Tb L_3 X-ray absorption edges of $Ce_{1-x}Tb_xO_{2-\delta}$ and Tb_4O_7 standard (with a formal valence of 3.5) with separate Tb^{3+} and Tb^{4+} features identified.

solid electrolytes (1.8×10^{-10} mol/s·cm^2 at 650 °C for $Bi_{0.60}Tb_{0.40}O_{1.5+\delta}$[18]) and slightly higher than that of Pr-substituted ceria [$J(O_2) = 1.9 \times 10^{-10}$ mol/s·cm].[23] However, ceria solid solutions are much more stable [till $p(O_2) = 10^{-19}$ atm at 700 °C, compared to $\sim 10^{-12}$ atm for bismuth solid solutions[11]] and may be used as oxygen

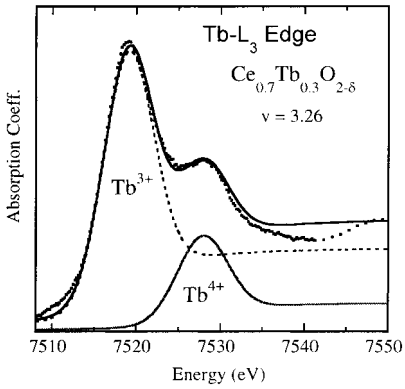

Figure 13. Tb L_3 edges of $Ce_{0.70}Tb_{0.30}O_{1.85+\delta}$ ($v_3 = 3.26$) along with the simulation of the separate Tb^{3+} and Tb^{4+} fitted features.

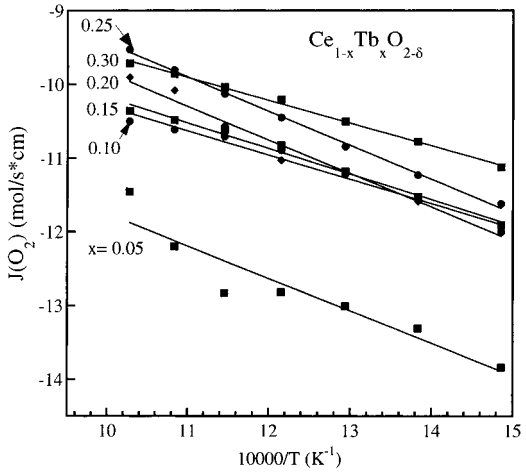

Figure 14. Temperature dependence of the oxygen permeability of the $Ce_{1-x}Tb_xO_{2-\delta}$ solid solutions.

membranes or solid electrolytes in an extended oxygen pressure range, which is a critical factor for potential technical application, e.g., in syngas production.[29] The total conductivity of the best conductive $Ce_{0.75}Tb_{0.25}O_{1.825+\delta}$ ($\sigma_{700°C} = 2.1 \times 10^{-2}$ S/cm) is 1−2 order of magnitude higher than that of the most commonly used solid electrolyte, stabilized zirconia ($\sigma_{700°C} < 10^{-3}$ S/cm), and close to that of the mixed conductors based on bismuth oxide at the corresponding temperature ($\sigma_{700°C} \sim 10^{-1}$ S/cm for $Bi_{0.85}Pr_{0.15}O_{1.925+\delta}$).[24]

Conclusion

$Ce_{1-x}Tb_xO_{2-\delta}$ ($x = 0-0.30$) solid solutions with the fluorite structure were prepared for the first time by the soft hydrothermal method using NH_4OH as mineralizer at 260 °C and ~10 MPa. Ultrafine particles of uniform crystallite dimension, ~35−40 nm can be formed in 20−40 min under hydrothermal conditions. Further heat treatment slowly increases the crystallinity of the powder from ~25 nm crystallite size in 30 min to ~35−40 nm in 12 h. Because of the small particle size of the ceria powder, the sintering temperature needed to obtain a dense ceramic pellet was reduced substantially from 1650 °C, that required for the ceria solid electrolytes prepared by conventional solid-state

(29) Mazanec, T. J. *Solid State Ionics* **1994**, *70/71*, 11.

methods, to ~1300 °C. The highest conductivity was found at $x = 0.25$ ($\sigma_{700°C} = 2.1 \times 10^{-2}$ S/cm, $E_a = 0.49$ eV) with electronic contribution to the total conductivity around 50% at 600−700 °C. The thermal expansion coefficients, determined from high-temperature X-ray data, are 11.8×10^{-6} K^{-1} for the CeO_2 and slowly decrease with increasing Tb substitution (10.8×10^{-6} K^- at $x = 0.30$). The oxide ion conductivity is 1−2 order of magnitude higher than that of the most commonly used solid electrolyte, stabilized zirconia, at corresponding temperatures ($\sigma_{650°C} \sim 10^{-3}$−$10^{-4}$ S/cm). The oxygen permeability, $J(O_2)$, calculated from ionic and electronic conductivies, systematically increases with increasing Tb substitution and temperature and is close to the oxygen permeability of the mixed conductors based on the best conductive bismuth oxide solid electrolytes [$J(O_2) = 2.9 \times 10^{-10}$ mol/s·cm at 700 °C for $Ce_{0.75}Tb_{0.25}O_{1.875+\delta}$].

CM980682D